

Direct Evidence of Spontaneous Abrikosov Vortex State in Ferromagnetic Superconductor $\text{EuFe}_2(\text{As}_{1-x}\text{P}_x)_2$ with $x = 0.21$

L. Ya. Vinnikov,¹ I. S. Veshchunov,^{2,3} S. Yu. Grebenchuk,³ D. S. Baranov,^{1,3,4} V. S. Stolyarov,^{1,3} V. V. Dremov,^{1,3} N. Zhou,⁵ Z. X. Shi,⁶ X. F. Xu,⁷ S. Pyon,² Yue Sun,^{2,8} Wenhe Jiao,⁹ Guanghan Cao,⁹ A. A. Golubov,³ D. Roditchev,⁴ A. I. Buzdin,¹⁰ and T. Tamegai²

¹*Institute of Solid State Physics, Russian Academy of Sciences, Chernogolovka, Moscow region, 142432 Russia*

²*Department of Applied Physics, The University of Tokyo, 7-3-1 Hongo, Bunkyo-ku, Tokyo 113-8656, Japan*

³*Moscow Institute of Physics and Technology (State University), Dolgoprudnyi, Moscow region, 141700 Russia*

⁴*Laboratoire de Physique et d'Etude des Matériaux LPEM-UMR8213 ESPCI-Paris, PSL Research University, INSP - Sorbonne Université, 10 rue Vauquelin, 75005 Paris, France*

⁵*Department of Physics and Key Laboratory of MEMS of the Ministry of Education, Southeast University, 211189 Nanjing, China*

⁶*School of Physics and Key Laboratory of MEMS of the Ministry of Education, Southeast University, 211189 Nanjing, China*

⁷*Department of Physics, Changshu Institute of Technology, Changshu 215500, People's Republic of China*

⁸*Institute for Solid State Physics, The University of Tokyo, 277-8581 Kashiwa, Japan*

⁹*Department of Physics, Zhejiang University, 310027 Hangzhou, China*

¹⁰*University Bordeaux, LOMA, F-33405 Talence, France*

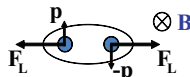
(Dated: September 4, 2022)

Using low-temperature Magnetic Force Microscopy (MFM) we provide direct experimental evidence for spontaneous vortex phase (SVP) formation in $\text{EuFe}_2(\text{As}_{0.79}\text{P}_{0.21})_2$ single crystal with the superconducting $T_{\text{SC}}^0 = 23.6$ K and ferromagnetic $T_{\text{FM}} \sim 17.7$ K transition temperatures. Spontaneous vortex-antivortex (V-AV) pairs are imaged in the vicinity of T_{FM} . Also, upon cooling cycle near T_{FM} we observe the first-order transition from the short period domain structure, which appears in the Meissner state, into the long period domain structure with spontaneous vortices. It is the first experimental observation of this scenario in the ferromagnetic superconductors. Low-temperature phase is characterized by much larger domains in V-AV state and peculiar branched striped structures at the surface, which are typical for uniaxial ferromagnets with perpendicular magnetic anisotropy (PMA). The domain wall parameters at various temperatures are estimated.

INTRODUCTION

The problem of the coexistence of superconducting and magnetic orderings has been one of the most puzzling enigmas for decades (see, e.g., Refs. 1, 2, 3 and 4 for reviews). One can separate two basic mechanisms responsible for the interaction of superconducting (SC) order parameter with magnetic moments in the ferromagnetic (FM) state: the electromagnetic interaction of Cooper pairs with magnetic field created by magnetic moments (orbital effect), which was first discussed by Ginzburg [5], and the exchange interaction of magnetic moments with electrons in Cooper pairs (paramagnetic effect), which tends to align the spins [6, 7] (See Fig. 1). In the case of orbital effect, superconductivity will be suppressed if the internal field B_{in} generated by the FM moments exceeds the critical magnetic field H_c for a Type-I, or the upper critical magnetic field H_{c2} for a Type-II, superconductor. But since the internal exchange energy in ferromagnets is usually significantly larger than the condensation energy of conventional superconductivity, the paramagnetic effect can easily destroy Cooper pairs in the spin singlet superconductor. Indeed, even a tiny amount of FM impurity in most superconductors leads to the destruction of SC [8, 9]. Consequently, strong magnetic moments destroy singlet Cooper pairs via the paramagnetic and orbital effects [4], making the coexistence of ferromagnetism and superconductivity a very rare phenomenon.

- Orbital effect (Lorentz force)



- Paramagnetic effect (Exchange interaction)

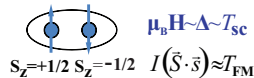


FIG. 1: The "Yin and Yang" of Ferromagnetism and Superconductivity.

For possible coexistence of these two seemingly incompatible and antagonistic FM and SC states various types of modification of the magnetic ordering, e.g. a cryptoferrimagnetic structure [10], domain structure [11] or a spiral magnetic structure [12, 13], have been discussed both theoretically and experimentally. The period of these structures is determined by the intrinsic parameters of the material such as the coherence length ξ , the London penetration depth λ , Fermi wave vector k_F . This period is normally smaller than ξ and λ and does not depend on the size and shape of the sample. For the cryptoferrimagnetic state the period of domain structure is found to be $(\xi/k_F^2)^{1/3} \ll \xi$, the period of the spiral magnetic structure is $(a_m \lambda)^{1/2} \ll \lambda$, with the magnetic length $a_m = J/M^2 a$, where J is the exchange constant, M is the magnetic moment and a is the interatomic distance [4, 14]. According to Sonin[15]: "Appearance of this structure means that ferromagnetism has lost competition with superconductivity and the superconducting ferromagnet is not a ferromagnet in a strict sense: this is an antiferromagnetic structure with a large but finite period".

Another way to make long-range FM ordering and SC coexist in the bulk material is to "switch off" the paramagnetic effect. It is possible either in materials with very weak exchange interaction between magnetic atoms and conducting electrons or when the Cooper pairs are in a spin-triplet state. The latter scenario is realized in a series of uranium compounds UGe_2 , URhGe and UCoGe , in which both superconductivity and ferromagnetism are believed to arise from the same types of electrons, and the Curie temperature T_{FM} is substantially higher than the superconducting critical temperature T_{SC} [16]. In this case, the main mechanism of the interplay between the two orders is the orbital effect. For a Type-II SC, in the single domain state with uniform magnetization M_s , vortices are predicted to appear spontaneously if the internal magnetic field B_{in} lies in the range $H_{c1} < B_{in} = 4\pi M_s < H_{c2}$, where H_{c1} is the lower SC critical magnetic field [12, 17–25]. In this spontaneous vortex phase (SVP), the flux density corresponds to the internal magnetic field B_{in} . Another situation was studied by Krey [26], who noted that the interaction between magnetic induction and superconductivity can cause an intrinsic domain structure generation. The Meissner state of such a ferromagnetic superconductor should be spatially inhomogeneous and consist of intrinsic Meissner domains forming a domain Meissner state (**DMS**). This DMS should have a short period, smaller than $\lambda(T)$, but also smaller than the period of the macroscopic magnetic domain structure (**DS**) of the same ferromagnet in the absence of superconductivity. Indeed, the DS in ferromagnets are usually related to demagnetization effect, and have a typical size of μm range. Later on Fauré and Buzdin [27, 28] predicted that the demagnetization effect should lead to the additional shrinkage of the DMS. The large concentration of the domain walls in DMS as compared with normal DS may lead to the subsequent transition into the spontaneous vortex-antivortex state, when the ferromagnetic domains carry a dense vortex lattice. The scenario of such DMS-DVS transition in zero external magnetic field was proposed in [27–29]. The period of this domain vortex state (**DVS**) is expected to be quite similar to the DS in a non-superconducting ferromagnet.

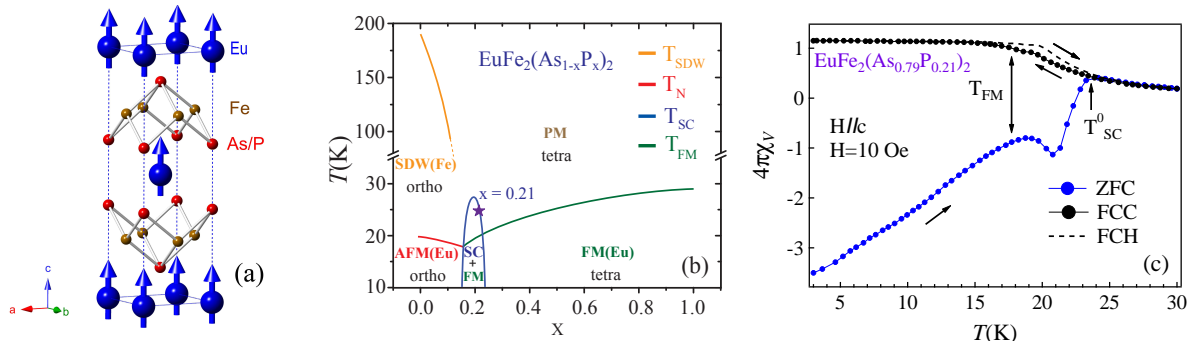


FIG. 2: (a) The body centered tetragonal chemical and magnetic unit cell of $\text{EuFe}_2(\text{As}_{1-x}\text{P}_x)_2$ with nearly optimal doping level $x_{\text{opt}} \sim 0.2$ (space group $I4/mmm$). The arrows denote the ordered Eu^{2+} magnetic moment directions in zero magnetic field. Only the Eu^{2+} spins are shown. P atoms occupy the As site. (b) The complex phase diagram for $\text{EuFe}_2(\text{As}_{1-x}\text{P}_x)_2$ as a function of P doping level, x (adopted from Ref. [31]). Note extremely narrow SC dome for this compound [32]. The minimum in the magnetic ordering temperature T_{Eu} near optimal doping level x_{opt} can be ascribed to the change of the sign and the strength of the indirect Ruderman-Kittel-Kasuya-Yosida (RKKY) exchange interaction in the Eu^{2+} sublattice (from antiferromagnetic (AFM) state to FM state with increasing x) [33, 34]. (c) Temperature dependence of the zero-field-cooled (ZFC), $H = 10$ Oe field-cooled FC magnetic susceptibility of $\text{EuFe}_2(\text{As}_{0.79}\text{P}_{0.21})_2$ single crystal upon cooling (FCC) and heating (FCH) cycles. FM transition temperature $T_{\text{FM}} \sim 18$ K and SC critical temperature $T_{\text{SC}}^0 = 23.6$ K (defined at zero resistivity) are marked by vertical arrows. The diamagnetic signal in ZFC susceptibility appears only below ~ 22 K ($< T_{\text{SC}}^0$), due to the dominant effect of strong paramagnetism of Eu^{2+} sub-lattice above T_{FM} .

In $\text{EuFe}_2(\text{As}_{1-x}\text{P}_x)_2$ with $x \sim 0.2$, a material becoming superconducting at $T_{\text{SC}} \sim 25$ K and ferromagnetic below $T_{\text{FM}} \sim 18$ K [30, 31], the coexistence of the two antagonistic phenomena becomes possible due to the extremely weak

exchange field produced by Eu^{2+} subsystem [35–38]. (The magnetic structure of the optimally doped compound and the phase diagram of the $\text{EuFe}_2(\text{As}_{1-x}\text{P}_x)_2$ system as a function of P/As substitution are presented in Figs. 2(a) and (b), respectively). So the main mechanism of the interplay between the two orders is the orbital effect. This provides the unique opportunity to test, in a direct MFM experiment, the long standing prediction of the spontaneous emergence of the flux-line lattice at zero field (SVP) and the domain structure in a ferromagnetic superconductor.

Experimental evidence for magnetic domains and SVP formation in $\text{EuFe}_2(\text{As}_{0.79}\text{P}_{0.21})_2$ single crystal

Single crystals of $\text{EuFe}_2(\text{As}_{0.79}\text{P}_{0.21})_2$ were grown using a self-flux method [39]. The actual chemical composition of the studied samples was determined using energy dispersive X-ray (EDX) analysis. Temperature dependences of the zero-field-cooled (ZFC) and field-cooled (FC) magnetic susceptibility of $\text{EuFe}_2(\text{As}_{0.79}\text{P}_{0.21})_2$ single crystal are presented in Fig. 2(c). FC susceptibility data show a thermal hysteresis near $T_{\text{FM}} \sim 18$ K below $T_{\text{SC}}^0 = 23.6$ K (determined by zero resistivity) upon cooling in magnetic field of $H = 10$ Oe (FCC cycle) with subsequent heating in the same field (FCH cycle), which is a signature of the first-order phase transition [40–42]. Further details of the sample characterizations will be given elsewhere.

MFM imaging was performed in a cryogenic microscope (Attocube Attodry 1000) using CoCr coated silicon cantilever with resonance frequency approximately 89 kHz, spring constant 2.8 N/m, quality factor up to ~ 1700 and coercive field of 1.4 kOe at 4 K (Bruker/MESP). All MFM images were taken in buffer helium gas atmosphere at pressure 5×10^{-1} mbar and at different temperatures with exceptional temperature stability and precision of 1 mK. The change of the scanning area vs temperature (the scanning area linearly grows with increasing temperature) was taken into account, the area of each scan was recalculated. Prior to MFM imaging the $\text{EuFe}_2(\text{As}_{0.79}\text{P}_{0.21})_2$ single crystal was cleaved in air, fixed to the sample holder with out-of-plane c -axis perpendicular to the scan directions and immediately transferred into the MFM chamber. Hereinafter MFM imaging of vortices and domains was performed in a lift mode at $\sim 70 - 110$ nm above the sample surface in order to avoid vortex and domain dragging by the magnetic tip. In this mode the MFM contrast is provided by the phase-shift in the cantilever oscillation.

Evolution of magnetic flux structure on the surface of $\text{EuFe}_2(\text{As}_{0.79}\text{P}_{0.21})_2$ single crystal of the thickness $d_F \sim 12$ μm after ZFC below Curie temperature T_{FM} K, at $T = 17.614$ K and at $T = 17.571$ K, and after FC in magnetic field of $H = 7$ Oe, at $T = 17.444$ K is shown in Figs. 3(a-b) and 3(c), respectively. The bright and dark parts in the images represent the magnetic domains/vortices with upward and downward magnetizations. Typical MFM phase-shift signal detected from single vortices in the temperature range just above the Curie temperature, at $T \gtrsim T_{\text{FM}}$ is about 0.3–0.5 deg. FM domains in the Meissner state are revealed in a rather narrow temperature interval below T_{FM} . Measured Meissner domain widths are $l \sim 220$ nm and $l \sim 130$ nm as indicated in cross sections in Figs. 3(b) and 3(c), respectively. Note that the detected MFM phase-shift signal above Meissner domains (DMS) is much smaller compared to the signal detected above domains in the mixed state with vortices (DVS). Remarkably, the neighbouring domains in DVS host quantum vortex of opposite flux orientations (vortices and antivortices, V-AVs). Thus, unlike in non-magnetic superconductors, in which the vortices penetrate from the sample edges, in ferromagnetic superconductor $\text{EuFe}_2(\text{As}_{0.79}\text{P}_{0.21})_2$ the V-AV pairs nucleate directly inside, at the domain walls, upon cooling below T_{FM} . Figs. 4(c-f) illustrate the generation of spontaneous V-AV pairs after cooling at zero magnetic field below Curie temperature down to $T_{\text{min}} = 4.16$ K with subsequent heating slightly above T_{FM} . Fig. 4(a) shows an absence of any notable magnetic flux structure at $T = 18.171$ K, i.e. just above the T_{FM} before cooling. However, upon heating up to T_{FM} , generated V-AVs remained trapped (due to pinning) at the positions of ferromagnetic domains with opposite polarities. At $T = 17.740 - 17.757$ K $\approx T_{\text{FM}}$ (Fig. 4(c-d)) ferromagnetic domains with an average size of $l \sim 1$ μm are still present as an MFM background with a notable overlaid MFM vortex contrast. As one can see in Figs. 4(b-f) magnetic domains transform into V-AV structures upon heating above T_{FM} . Importantly, the sign of the induced V-AVs corresponds to the sign of disappearing (smearing) magnetic domains, V-AVs are aligned along these domains. Above $T = 19$ K most of the V-AV pairs annihilate.

DOMAINS IN MEISSNER/VORTEX STATES (DMS/DVS) [27, 28]

For spatially separated FM/SC system coupled only by the magnetic field below T_{SC} of the SC layer in the Meissner state the shrinkage of domains in FM layer with PMA is small, up to a factor $(3/2)^{1/2}$ given by Sonin [43]. However, in a bulk ferromagnetic superconductor depending on parameters $\lambda(T)$, \tilde{w} , d_F , where \tilde{w} is an effective width of the domain wall, d_F is the thickness of the FM superconductor, this shrinkage of domain width l in the Meissner state can be much more significant [27].

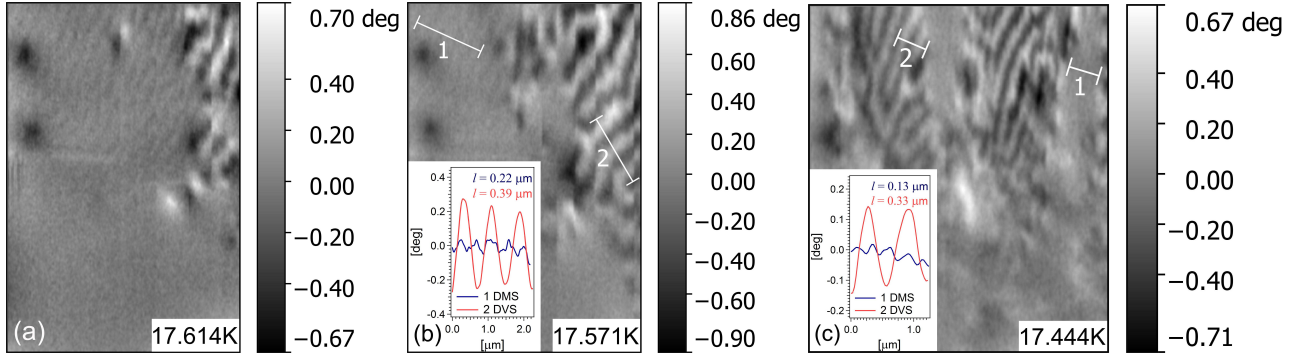


FIG. 3: The transition between the Meissner FM domain state (DMS) and mixed (V-AV) FM domain state (DVS) upon cooling below T_{FM}^* (the temperature at which the domain structure is first observed) after ZFC (a) at $T = 17.614$ K (b) at $T = 17.571$ K and (c) after FC in magnetic field of $H = 7$ Oe at $T = 17.444$ K. The scanning area for (a) and (b) MFM images is $7.2 \times 10.8 \mu\text{m}^2$. The scan height is ~ 70 nm. The scanning area for (c) MFM image is $11.7 \times 13.5 \mu\text{m}^2$. The scan height is ~ 100 nm.

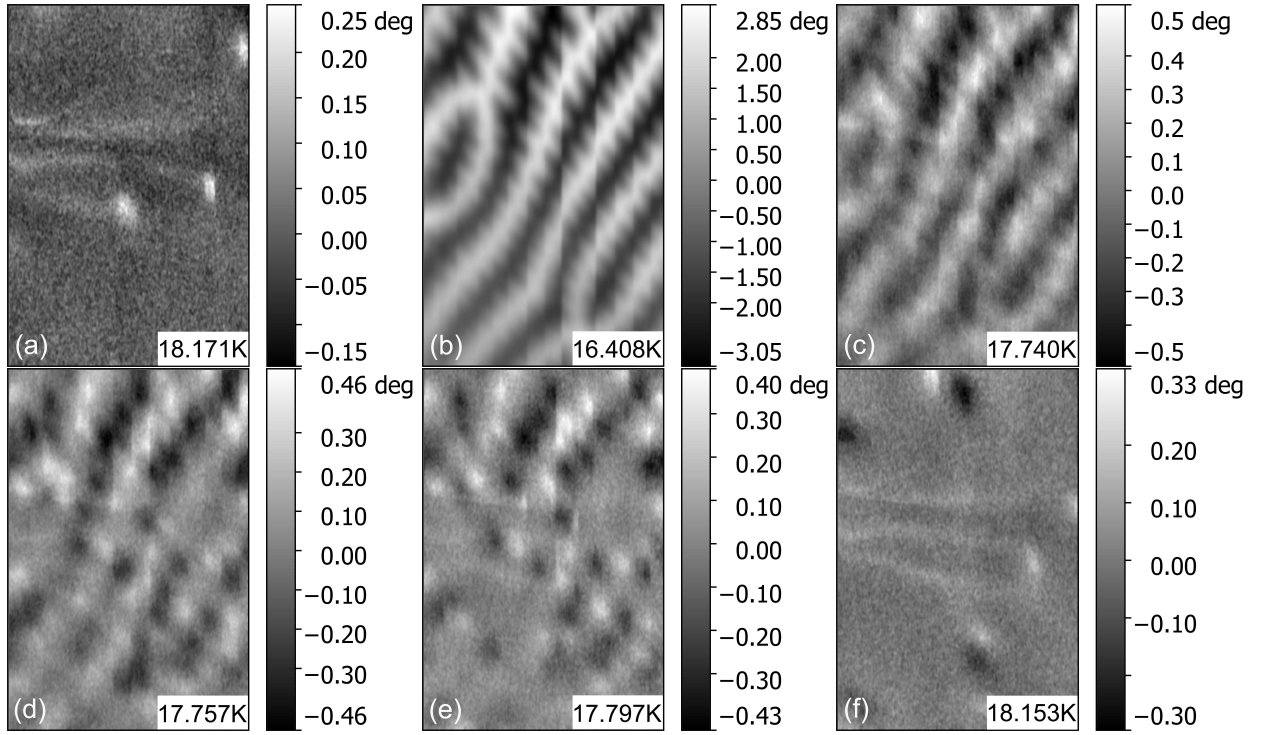


FIG. 4: Generation of spontaneous vortex-antivortex (V-AV) pairs in $\text{EuFe}_2(\text{As}_{0.79}\text{P}_{0.21})_2$ single crystal. MFM phase-shift signal images (a) upon cooling from $T_{SC}^0 = 23.6$ K at zero field, taken at $T = 18.171$ K; (b) upon heating from $T_{\min} = 4.16$ K, well below Curie temperature $T_{FM}^* \sim 17.7$ K, and taken at $T = 16.408$ K; (c) 17.740 K; (d) 17.757 K; (e) 17.797 K; (f) 18.153 K. The scanning area for all images is $7.2 \times 10.8 \mu\text{m}^2$. The scan height is ~ 70 nm.

Following the result of Fauré and Buzdin [27], the energy of domain structure in the Meissner state per unit area of the ferromagnetic superconductor depends on the domain width l as

$$E_{DMS} = M_s^2 \frac{l_N^2}{\lambda} \left\{ \frac{2\pi\lambda d_F}{l_N^2} \left[1 - \frac{2}{\pi \tilde{l}} \tanh\left(\frac{\pi \tilde{l}}{2}\right) \right] + \frac{32 \lambda^2}{\pi l_N^2} \tilde{l} \sum_{k=0}^{\infty} \frac{2k+1}{[\tilde{l}^2 + (2k+1)^2]^{3/2} [2k+1 + \sqrt{\tilde{l}^2 + (2k+1)^2}]} \right. \\ \left. + \frac{14\zeta(3)}{\pi^3} \frac{1}{\tilde{l}} \right\},$$

where l_N is the characteristic domain width in the normal (non-superconducting) state (*e.g.* in overdoped $\text{EuFe}_2(\text{As}_{1-x}\text{P}_x)_2$ single crystal with $x > 0.25$), and \tilde{l} is the dimensionless domain width, $\tilde{l} = \frac{l}{\pi\lambda}$. The last term is the contribution of the domain wall energy (specific wall energy) $M_s^2\tilde{w}$, which is assumed to be the same in the Meissner and normal states. The domain width in the normal phase l_N is determined by the trade-off between demagnetization (stray field) energy $\propto lM_s^2$ and domain wall surface energy $M_s^2\tilde{w}d_F/l$, using the following relationship $l_N = \sqrt{d_F\tilde{w}\sqrt{\pi^2/14\zeta(3)}}$ [27, 46]. In the superconducting Meissner state the energy balance also includes the kinetic energy of currents which are spontaneously generated to screen the rising magnetic field in alternating up- and down- domains, making l smaller than l_N . On the other hand, in the mixed (V-AV) state when $4\pi M_s \gg H_{c1}$ the energy of the domain structure (and thus the period of DVS) is basically the same as in the normal phase [29], and we consider $l_{DVS} \sim l_N$. In superconducting iron pnictides typical $\lambda(0) \sim 200 - 300$ nm [44] and close to $T_{\text{FM}} \sim 17.7$ K for this crystal estimated $\lambda(\sim T_{\text{FM}}) \sim 400 - 500$ nm [45]. Thus, measured Meissner domain widths in $\text{EuFe}_2(\text{As}_{0.79}\text{P}_{0.21})_2$ upon cooling below T_{FM} (Figs. 3(b) and 3(c)) are smaller than $\lambda(\sim T_{\text{FM}})$. With known thickness of the crystal $d_F \sim 12$ μm , and corresponding period of the domain structure in the mixed state revealed by MFM at $T = 17.571$ K (Fig. 3(b)), $l_{DVS} \sim 0.39$ μm , one can also estimate the effective domain wall width \tilde{w} at the DMS-DVS phase transition using the formula for $l_{DVS} \sim l_N$, and we get $\tilde{w} \sim 21$ nm. Then for our ferromagnetic superconductor $\text{EuFe}_2(\text{As}_{0.79}\text{P}_{0.21})_2$, we can estimate the domain width in the Meissner state as $l_{DMS} \propto (\tilde{w}\lambda^2)^{1/3}$, which corresponds to the minimum of $E_{DMS}(\tilde{l})$ in the limit $\lambda \ll (\tilde{w}d_F^3)^{1/4}$ (see Ref. 27). For $\lambda(\sim T_{\text{FM}}) \sim 400-500$ nm, $\tilde{w} \sim 21$ nm, we find $l \sim 150-180$ nm, and it is rather close to experimental data (Fig. 3(a-b)). The domain wall width in $\text{EuFe}_2(\text{As}_{0.79}\text{P}_{0.21})_2$ at temperatures well below T_{FM} , can be estimated as follows. For the ferromagnet with uniaxial perpendicular anisotropy K_u , in-plane saturation field is $H_{\text{sat}}^{/ab} = 2K_u/M_s$. According to Nandi *et al.* [47] in-plane saturation field in $\text{EuFe}_2(\text{As}_{1-x}\text{P}_x)_2$ with $x = 0.15$ is $H_{\text{sat}}^{/ab} \sim 6$ kOe. For magnetic sublattice consisting of the S-state Eu^{2+} ions with the electron spin $S = 7/2$ and the magnetic moment $m_{\text{at}}/\text{Eu}^{2+} = 7\mu_B$ [47], the low-temperature saturation magnetization in $\text{EuFe}_2(\text{As}_{0.79}\text{P}_{0.21})_2$ can be evaluated as $M_s \sim 714$ G. Then we find $K_u \sim 2.1 \times 10^6$ erg/cm³ and low-temperature quality factor $Q = K_u/2\pi M_s^2 \sim 0.67$, which is close to that of cobalt [46]. Note that in $\text{EuFe}_2(\text{As}_{0.79}\text{P}_{0.21})_2$ the domain width in the mixed state is increasing at low temperatures. Low-temperature DVS is characterized by much larger domains and peculiar branched striped structures [46, 48] with the measured $l_{DVS} \sim 0.5$ μm at $T_{\text{min}} = 4.16$ K. The increase of the domain wall energy in $\text{EuFe}_2(\text{As}_{0.79}\text{P}_{0.21})_2$ single crystal is probably larger than the increase of magnetostatic energy upon cooling, which can explain the observed expansion of domains in the mixed state at low temperatures [49]. Using the same formula for $l_{DVS} \sim l_N$, the effective domain wall width at low temperatures can be estimated as $\tilde{w} \sim 35$ nm. With the following expressions for Bloch domain wall width $\delta = \pi\sqrt{(A/K_u)}$ and specific domain wall energy $\Delta = \frac{4}{\pi}\delta K$ [46], we can find the relation between \tilde{w} and δ , $\tilde{w} = 8 \times Q \times \delta$. For obtained quality factor $Q \sim 0.67$ we can estimate Bloch domain wall width as $\delta \sim 6.5$ nm and evaluate the exchange stiffness constant as $A \sim 0.9 \times 10^{-7}$ erg/cm.

Note that the temperature dependence of the Meissner domain width in $\text{EuFe}_2(\text{As}_{0.79}\text{P}_{0.21})_2$ near T_{FM} shows clear hysteretic behaviour. Narrow Meissner domains with $l \sim 130 - 220$ nm during cooling cycle (Fig. 3) transform into wide domains $l \sim 0.6-1$ μm after heating from T_{min} (Fig. 4(b)). Also, Meissner domains appear at lower temperatures during cooling process at $T \sim 17.6$ K, but survive at slightly higher temperatures upon heating at $T \sim 17.8$ K with trapped V-AVs. To obtain the equilibrium domain structures hindered by the increasing (mutual) pinning of domain walls and spontaneous V-AVs it is necessary to apply an alternating perpendicular magnetic field with decaying amplitude [49]. Thermal hysteresis in the domain structure formation between cooling and heating cycles can be attributed to the first-order phase transition, as evidenced by magnetic susceptibility measurements (Fig. 2(c)).

CONDITION FOR CREATION OF VORTEX-ANTIVORTEX PAIRS AT DMS-DVS TRANSITION [28, 29]

According to Refs. 28, 29 in the case of large magnetic domain width l and rather good screening of magnetic field, $l \gg \lambda$, SVP exists if the internal magnetic field generated by the magnetization M_s satisfies the condition, $H_{c1} < 4\pi M_s < H_{c2}$. In the opposite limit of narrow domains $l \ll \lambda$, the internal magnetic field $4\pi M_s$ needed for generation of SVP is much larger than H_{c1} . Following the results of Dao *et al.* [28] and Khaymovich *et al.* [29] we can estimate the threshold magnetization M_{th} for the transition between DMS and DVS. According to Ref. [28] at $M > M_{th}$, the energy for the creation of the vortex-antivortex (V-AV) pair in the middle of adjacent domains becomes negative. This energy is the sum of (i) the energy decrease when (anti)vortices are driven by screening currents away from domain boundaries to domain centers and (ii) the increase of the interaction energy between one vortex and its antivortex as they move apart from each other. The magnetization threshold for narrow domains $l \ll d_F$, $l \ll \lambda$ in the case of weak vortex pinning and small Bean-Livingston barrier, takes the form:

$$4\pi M_{th} = \frac{2\Phi_0 \ln(l/\xi)}{\pi l^2}, l \ll d_F, \lambda \quad (1)$$

One can see from the expression for M_{th} that the intervortex spacing within ferromagnetic domains at the DMS-DVS transition is comparable to the domain width l . Using the formula for the Meissner domain width obtained in Ref. 27, $l \propto (\tilde{w}\lambda^2)^{1/3}$ and $M_{th} \propto H_{c1} \frac{\lambda^2}{l^2}$, we find $M_{th} \propto H_{c1} (\frac{\lambda}{\tilde{w}})^{2/3}$. Thus, the internal magnetic field $4\pi M_{th}$ needed for generation of V-AV pairs is much larger than H_{c1} , $4\pi M_{th} \gg H_{c1}$ since $\lambda \gg \tilde{w}$. Indeed, upon cooling and heating cycles the observed intervortex distances within ferromagnetic domains in Fig. 3(a-b) and in Fig. 4(d-e) are comparable to the Meissner domain widths $l \sim 220$ nm and $l \sim 1$ μ m, respectively. In Fig. 3(c) the width of Meissner domains prior to the DMS-DVS transition is too small $l \sim 130$ nm, and individual V-AVs within DVS can not be resolved with MFM. For the average domain width in the Meissner state upon cooling cycle $l_{DMS} = 180$ nm, $\xi_{ab}(\sim T_{FM}) \sim 10$ nm, the transition from DMS to DVS occurs at the magnetization threshold $M_{th} \approx 90$ G and corresponding internal magnetic field $B_{in} = 4\pi M_{th} \approx 1.1$ kG (thus, $B_{in} \gg H_{c1}$ at $T \sim T_{FM}$). In accordance with muon-spin rotation (μ SR) and neutron diffraction measurements on polycrystalline $\text{EuFe}_2(\text{As}_{1-x}\text{P}_x)_2$ with $x = 0.2$ and single crystals with $x = 0.19$, the saturation magnetization just below T_{FM} increases rather fast, as $M_s(T) = M_s(0)(1 - T/T_{FM})^\delta$ with the exponent $\delta \sim 0.36 - 0.5$ [50–52]. The internal magnetic field at low temperatures in $\text{EuFe}_2(\text{As}_{0.79}\text{P}_{0.21})_2$ is $B_{in}(0) \approx 9$ kG [47] and then we can roughly estimate the temperature T_1 of the first-order transition from DMS to DVS as

$$\frac{T_{FM} - T_1}{T_{FM}} \sim \left(\frac{B_{in}}{B_{in}(0)} \right)^2 \sim 1.6 \cdot 10^{-2}$$

For $T_{FM} = 17.7$ K, we find $T_{FM} - T_1 \sim 0.3$ K. Thus, estimation of $T_1 \sim 17.4$ K shows fair agreement with our experimental results. Note that a decrease in domain width l results in a broader temperature interval of the DMS existence. The agreement between the theory and experiment is impressive both in the determination of the Meissner domain width and the temperature of the DMS-DVS phase transition. With such a narrow phase window of the DMS, only precise temperature control permitted us to observe this elusive DMS-DVS transition in $\text{EuFe}_2(\text{As}_{0.79}\text{P}_{0.21})_2$ single crystal.

CONCLUDING REMARKS

To summarize, studies of magnetic flux structures in europium-based iron pnictides continue to be amazing. Using low-temperature MFM, striped magnetic domain structures are revealed in $\text{EuFe}_2(\text{As}_{1-x}\text{P}_x)_2$ single crystal with nearly optimal doping level $x = 0.21$ in the superconducting state with $T_{SC}^0 = 23.6$ K, well below Curie temperature $T_{FM} = 17.7$ K, which means the ability of the coexistence of SC and FM orders on an atomic scale [48]. Thus, the spin glass state, proposed in Ref. 33 can be ruled out for the studied $\text{EuFe}_2(\text{As}_{0.79}\text{P}_{0.21})_2$ single crystal. The transition from narrow Meissner domains (DMS) to the mixed state domains (DVS) with longer period is observed upon cooling below T_{FM} . Note that in the non-superconducting analogous compound, e.g. overdoped $\text{EuFe}_2(\text{As}_{1-x}\text{P}_x)_2$ single crystal of similar thickness, only large domains with $l = l_N$ are expected just below T_{FM} . Spontaneous V-AV pairs are revealed after cooling FM superconductor $\text{EuFe}_2(\text{As}_{0.79}\text{P}_{0.21})_2$ in zero magnetic field below T_{FM} with subsequent heating slightly above FM transition temperature. Vortices and antivortices remain trapped at the positions of FM domains with opposite polarities. Above $T = 19$ K, still below T_{SC}^0 , most of the V-AV pairs annihilate. The possibility of formation and visualization of spontaneous V-AVs within branched stripe-like domains at lower temperatures with higher magnetic flux density $4\pi M_s \sim 9$ kG remain as open questions and require further studies. High-resolution scanning tunneling microscopy (STM) should be employed.

It is worth noting that the coexistence of SC (with $T_{SC} = 36$ K) and FM (with $T_{FM} = 15$ K) was discovered recently in polycrystalline $\text{RbEuFe}_4\text{As}_4$ [53, 54] and in $\text{CsEuFe}_4\text{As}_4$ [53, 55], ordered, stoichiometric, iron-based superconductors of 1144-type [56]. Single crystals of CaK-1144 iron-based superconductor have been successfully grown and characterized [57]. We expect that the temperature range in which spontaneous V-AVs and Meissner domains may exist in RbEu -1144 or CsEu -1144 single crystals will be broader than that of 122-type europium based FM superconductors. Another possibility to increase the temperature interval of the DMS existence is to reduce T_{FM} by substituting Eu^{2+} in $\text{EuFe}_2(\text{As}_{1-x}\text{P}_x)_2$ with non-magnetic ions, e.g. Sr^{2+} of similar size [58, 59].

Since the domain width in the Meissner state can be greatly reduced compared to that of non-superconducting ferromagnets $l_{DMS} \ll l_N$, we anticipate rapid growth of the field of FM superconductors in the near future and the development of new 'superconducting ferromagnetic domain-memory'.

Acknowledgments

We would like to thank V.V. Ryazanov, L.S. Uspenskaya, A.S. Mel'nikov and S.V. Mironov for useful discussions and E.Yu. Postnova, A.G. Shishkin, L.G. Isaeva for experimental assistance. This work is supported by the National Science Foundation of China (No. 11474252, 11611140101 and U1432135). The MFM studies were supported by the Ministry of Education and Science of the Russian Federation (project No. 14.Y26.31.0007).

Supplementary: Magnetic domains in normal state

Domain theory postulates the existence of large regions of uniform magnetization in a macroscopic sample, which are separated by planar regions - the domain walls - where the magnetization rotates from one easy direction to another. An applied field changes the net magnetization of the sample by causing the walls to move, thus making the magnetization in the domains rotate towards the applied field direction. The magnetostatic energy depends on the wall positions and the domain orientations. The reason for the existence of domains is that the magnetostatic energy is greatly reduced [46, 60–62].

Lets determine the energy of the magnetic field near the surface of a ferromagnetic crystal at which plane-parallel domains perpendicular to the surface without change in the direction of magnetisation Fig.(5a). We will show below how the magnetostatic energy is reduced by the appearance of domains.

In the magnetostatic limit, no time dependence or conduction currents are involved, and Maxwell's equations are then:

$$\nabla \times \mathbf{H} = 0, \quad \nabla \cdot \mathbf{B} = 0 \quad (2)$$

Magnetic scalar potential can be defined as

$$\mathbf{H} = -\text{grad } \varphi_m = -\nabla \varphi_m \quad (3)$$

same as in electrostatics for single "charge" m :

$$\varphi_m = \frac{m}{r} \quad (4)$$

and magnetostatic energy of the system of "charges" is given by:

$$U = \frac{1}{2} \sum_i m_i \varphi_{mi} \quad (5)$$

Using $\mathbf{B} = (\mathbf{H} + 4\pi\mathbf{M})$, and $\mathbf{H} = -\nabla\varphi_m$ it follows that $-\nabla^2\varphi_m + 4\pi\nabla\cdot\mathbf{M} = 0$, hence the magnetic scalar potential obeys Poisson's equation, where the volume magnetic charge density $\rho_m = -\nabla\cdot\mathbf{M}$:

$$\nabla^2\varphi_m = -4\pi\rho_m \quad (6)$$

The boundary condition for \mathbf{B} at the surface of a ferromagnetic material (subscript 1) in air (subscript 2) is

$$\mathbf{B}_1^n = \mathbf{H}_1^n + 4\pi\mathbf{M} = \mathbf{B}_2^n = \mathbf{H}_2^n \quad (7)$$

hence $\mathbf{H}_1 \cdot \mathbf{e}_n - \mathbf{H}_2 \cdot \mathbf{e}_n + 4\pi\mathbf{M} \cdot \mathbf{e}_n = 0$. In terms of the magnetic scalar potential φ_m :

$$\frac{\partial\varphi_{m1}}{\partial r_n} - \frac{\partial\varphi_{m2}}{\partial r_n} = 4\pi\mathbf{M} \cdot \mathbf{e}_n \quad (8)$$

The change in derivative of the scalar potential φ_m at the surface is therefore equal to the surface magnetic charge density $\sigma_m = \mathbf{M} \cdot \mathbf{e}_n$. Given $\mathbf{M}(\mathbf{r})$, there is a unique solution of Eq. (6) and Eq. (8) for φ_m . If we know $\mathbf{M}(\mathbf{r})$ we

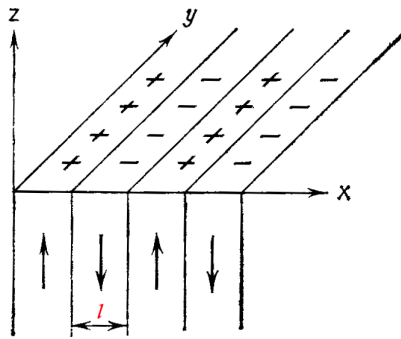


FIG. 5: Considered plate-like, stripe-like or laminated domain structure [61].

can calculate $\mathbf{H}(\mathbf{r})$. The converse is not possible; $\mathbf{M}(\mathbf{r})$ cannot be obtained from a knowledge of $\mathbf{H}(\mathbf{r})$, which, in any case, we can normally measure only outside the sample.

The problem of determining the magnetic field near such a surface is equivalent to the electrostatic problem of the field due to a plane divided into strips charged alternately positively and negatively with surface charge density or $\sigma_m = \pm M$.

Let the surface of the crystal be the plane $z = 0$, and let the x -axis be perpendicular to the plane of the domains. Domains with magnetization M along the $+z$ or $-z$ direction are separated by 180° walls lying parallel to the yz plane. Assume that the crystal extends indefinitely in the $-z$ and also in the $\pm x$ and $\pm y$ directions. The "surface charge density" $\sigma_m(x)$ is a periodic function with period $2l$ (l being the width of the domains), and its value in a typical period is $\sigma_m = -M$ for $-l < x < 0$, $\sigma_m = +M$ for $0 < x < l$ or: $\sigma_m = -M$ for $(2k+1)l < x < 2(k+1)l$ and $\sigma_m = +M$ for $2kl < x < (2k+1)l$, where k is an index that numbers the domains. We can represent this periodic step function in Fourier series:

$$\sigma_m(x) = \sum_{k=0}^{\infty} c_k \sin \frac{(2k+1)\pi x}{l}, \quad c_k = 4M/(2k+1)\pi \quad (9)$$

In all space other than at the crystal surface, where magnetic free poles exist, the magnetic potential must satisfy the Laplace equation:

$$\frac{\partial^2 \varphi_m}{\partial x^2} + \frac{\partial^2 \varphi_m}{\partial z^2} = 0 \quad (10)$$

because in this model the magnetic potential (or magnetic field \mathbf{H}) is constant along y -axis. The boundary condition Eq. (8) at $z = 0$ can be rewritten as

$$-\left[\frac{\partial \varphi_m}{\partial z} \right]_{z=0+} + \left[\frac{\partial \varphi_m}{\partial z} \right]_{z=0-} = 4\pi\sigma_m \quad (11)$$

We assume that magnetic field is created by the "charges" confined to the $z = 0$ plane, then the field and z -derivative of the potential φ_m must be symmetrical with respect to this plane:

$$\left[\frac{\partial \varphi_m}{\partial z} \right]_{z=0+} = - \left[\frac{\partial \varphi_m}{\partial z} \right]_{z=0-} \quad (12)$$

then final boundary condition can be written:

$$\left[\frac{\partial \varphi_m}{\partial z} \right]_{z=0-} = 2\pi\sigma_m \quad (13)$$

bearing in mind Eq. (9) we seek the solution of the Laplace equation $\varphi_m(x, z)$ as a series:

$$\varphi_m(x, z) = \sum_{k=0}^{\infty} b_k \sin \frac{(2k+1)\pi x}{l} e^{\mp(2k+1)\pi z/l} \quad (14)$$

where the two signs in the exponent relate to the half-spaces $z > 0$ and $z < 0$, $\varphi_m(x, z)$ must be decaying. The coefficients b_k are given by the boundary condition Eq. (13), hence $b_k = 2lc_k/(2k+1)$.

The magnetostatic energy is given by Eq. (5) and it can be calculated as the integral $\frac{1}{2} \int \sigma_m \varphi_m(x, z) df$ over the "charged" surface $z = 0$. The energy per unit area of the crystal surface:

$$F_D = U_m = \frac{1}{2} \frac{1}{2l} \int_{-l}^{+l} [\sigma_m \varphi_m(x, z)]_{z=0} dx = \frac{1}{4} \sum_{k=0}^{\infty} c_k b_k = \frac{8lM^2}{\pi^2} \sum_{k=0}^{\infty} \frac{1}{(2k+1)^3} = \frac{7lM^2}{\pi^2} \zeta(3) \quad (15)$$

The most common form of the Riemann zeta function:

$$\zeta(s) = \sum_{k=1}^{\infty} \frac{1}{k^s} = \sum_{k=1}^{\infty} \frac{1}{(2k)^s} + \sum_{k=0}^{\infty} \frac{1}{(2k+1)^s} \quad (16)$$

$$\sum_{k=1}^{\infty} \frac{1}{k^s} = 2^s \sum_{k=1}^{\infty} \frac{1}{(2k)^s} \quad (17)$$

then

$$\sum_{k=0}^{\infty} \frac{1}{(2k+1)^s} = \left(1 - \frac{1}{2^s}\right) \sum_{k=1}^{\infty} \frac{1}{k^s} \quad (18)$$

With the zeta function $\zeta(3) = 1.202$, the result of Eq. (15) is equal to $0.852 lM^2$ [63].

We see that the magnetostatic energy is greatly reduced by mixing N and S poles more closely. We find that the magnetostatic energy is proportional to the width of the domains, l . A decrease in l , therefore, results in a decrease in the magnetostatic energy, because the N and S poles are mixed more densely.

Magnetostatic energy per unit volume of the crystal is $0.852 \frac{lM^2}{d_F}$. This energy is less by a factor l/d_F than the magnetostatic energy in a single-domain structure. However, the domain walls increase the energy. The total domain wall area d_F/l is increasing with the process of splitting into domains.

The width of the domains in the crystal of the thickness d_F can be found by minimizing the sum $1.7 lM^2 + \Delta d_F/l$, the first term being the magnetostatic energy of domains Eq. (15) on both sides of the crystal and the second term the domain wall energy per unit area (surface) of the crystal, the energy per unit domain wall area (the specific wall energy) is Δ . Hence $l \sim 0.8 \frac{\sqrt{\Delta d_F}}{M}$.

We can calculate the domain wall energy using a simplified model when the spins change their direction in steps of equal angle from $\theta = 0$ to 180° over N atomic layers (the rotation of spin occurs at a constant rate) for a simple cubic lattice with lattice constant a . The angle θ_{ij} between spins on the neighbouring two layers is given by π/N . Since the number of atoms in a unit area of one layer is given by $1/a^2$, the number of nearest neighbour spin pairs in a unit area of the wall is given by N/a^2 , so that the exchange energy stored in a unit area of the domain wall is

$$\varepsilon_{ex} = \frac{N}{a^2} JS^2 \theta_{ij}^2 = \frac{JS^2 \pi^2}{a^2 N} = \frac{\pi^2 A}{2aN} \quad (19)$$

The exchange energy is inversely proportional to the thickness of the wall $\delta = Na$. The thicker the wall, the smaller the exchange energy, where $A = \frac{2JS^2}{a}$ is exchange stiffness constant.

On the other hand, the direction of each spin in the wall deviates from the easy axis, so that anisotropy energy is increased in the wall. The anisotropy energy density is increased by the anisotropy constant K when a spin rotates from the easy axis to the hard axis. In this simple model, the volume of the wall per unit area is given by $(N/a^2)a^3 = Na$, so that the anisotropy energy stored in a unit area of the domain wall is

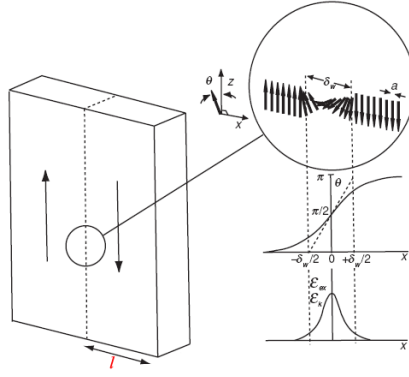


FIG. 6: The structure of the 180° Bloch domain wall [62].

TABLE I: Domain wall parameters for different ferromagnetic materials [62].

Ferromagnet	M_s (MA m ⁻¹)	A (pJ m ⁻¹)	K_1 (kJ m ⁻³)	δ nm	Δ (mJ m ⁻²)	Q
Ni ₈₀ Fe ₂₀	0.84	10	0.15	2000	0.01	
Fe	1.71	21	48	64	4.1	
Co	1.44	31	410	24	14.3	0.3
CoPt	0.81	10	4900	4.5	28.0	12
Nd ₂ Fe ₁₄ B	1.28	8	4900	3.9	25	4.8
SmCo ₅	0.86	12	17200	2.6	57.5	37
CrO ₂	0.39	4	25	44.4	1.1	
Fe ₃ O ₄	0.48	7	-13	72.8	1.2	
BaFe ₁₂ O ₁₉	0.38	6	330	13.6	5.6	3.6
EuFe ₂ (As _{0.79} P _{0.21}) ₂	0.71	0.9	210	6.5	1.7	0.7

$$\varepsilon_k = KNa \quad (20)$$

The thicker the wall, the larger the anisotropy energy. The equilibrium thickness is obtained by minimizing the total energy $\varepsilon_{tot} = \varepsilon_{ex} + \varepsilon_k$: $\frac{\partial \varepsilon_{tot}}{\partial N} = 0$, then $N = \frac{\pi}{a} \sqrt{\frac{A}{2K}}$, therefore the thickness of the wall $\delta = Na = \pi \sqrt{\frac{A}{2K}}$ and the total energy of the wall per unit area $\Delta = \varepsilon_{tot} = \pi \sqrt{2AK}$.

More accurate solution of the model in which the orientation of each spin in the wall is determined so as to minimize the total energy gives for 180° Bloch domain wall width:

$$\delta = \pi \sqrt{\frac{A}{K}} \quad (21)$$

and for the energy per unit 180° Bloch domain wall area:

$$\Delta = 4\sqrt{AK} \quad (22)$$

$\Delta = \frac{4}{\pi} \delta K$, then $l \sim 0.87 \sqrt{\frac{\delta K d_F}{M}}$, hence $l \propto \sqrt{\delta d_F}$. Domain wall parameters for different ferromagnetic materials are collected in Table (I). For EuFe₂(As_{0.79}P_{0.21})₂ single crystal we obtain $l \sim 1.78 \sqrt{\delta d_F}$.

Note that with increasing temperature Bloch wall profiles change via elliptical walls to linear domain walls (LDW) with the change of the modules of magnetization M rather than rotation of M close to T_{FM} [64].

[1] A.D. Huxley, *Ferromagnetic superconductors* Physica C **514**, 368 (2015); C.T. Wolowiec, B.D. White, and M.B. Maple, *Conventional Magnetic Superconductors* Physica C **514**, 113 (2015).

- [2] *Superconductivity and Magnetism*, edited by M.B. Maple and Ø. Fisher (Springer-Verlag, Berlin, 1982).
- [3] J. Flouquet and A. Buzdin, *Ferromagnetic superconductors* Phys. World **15**, 41 (2002).
- [4] L.N. Bulaevskii, A.I. Buzdin, M.L. Kulić, and S.V. Panjukov, *Coexistence of superconductivity and magnetism theoretical predictions and experimental results* Advances in Physics **34**:2, 175 (1985); A. Buzdin and J. Flouquet, *Magnetic Superconductors*, in Handbook of Magnetism and Advanced Magnetic Materials. Edited by H. Kronmüller and S. Parkin. Volume 1: Fundamentals and Theory. (2007) John Wiley & Sons, Ltd.; M.L. Kulić and A.I. Buzdin, *Coexistence of Singlet Superconductivity and Magnetic Order in Bulk Magnetic Superconductors and SF Heterostructures*, in J.B. Ketterson and S.N. Song, Superconductivity, (Cambridge University Press, Cambridge, 1999).
- [5] V.L. Ginzburg, *Ferromagnetic superconductors* Zh. Éksp. Teor. Phys. **31**, 202 (1956) [Sov. Phys. JETP **4**, 153 (1957)].
- [6] A.Yu. Aladyshkin, A.I. Buzdin, A.A. Fraerman, A.S. Mel'nikov, D.A. Ryzhov, and A. V. Sokolov, *Domain-wall superconductivity in hybrid superconductor-ferromagnet structures* Phys. Rev. B **68**, 184508 (2003).
- [7] A.I. Buzdin and A.S. Mel'nikov, *Domain wall superconductivity in ferromagnetic superconductors* Phys. Rev. B **67**, 020503 (R) (2003).
- [8] B.T. Matthias, H. Suhl, and E. Corenzwit, *Spin exchange in superconductors* Phys. Rev. Lett. **1**, 92 (1958).
- [9] A.A. Abrikosov, and L.P. Gor'kov, *Contribution to the theory of superconducting alloys with paramagnetic impurities* Zh. Eksp. Teor. Fiz **39**, 1243 (1960).
- [10] P.W. Anderson and H. Suhl, *Spin alignment in the superconducting state* Phys. Rev. **116**, 898 (1959).
- [11] S.K. Sinha, H.A. Mook, D.G. Hinks, and G.W. Crabtree, *Study of coexistence of ferromagnetism and superconductivity in single-crystal $ErRh_4B_4$* Phys. Rev. Lett. **48**, 950 (1982).
- [12] E.I. Blount and C.M. Varma, *Electromagnetic Effects near the Superconductor-to-Ferromagnet Transition* Phys. Rev. Lett. **42**, 1079 (1979); M. Tachiki, A. Kotani, H. Matsumoto, H. Umezawa, *Spin-spiral ordering in magnetic superconductor* Solid State Commun. **31**, 927 (1979).
- [13] J.W. Lynn, J.A. Gotaas, R.W. Erwin, R.A. Ferrel, J. K. Bhattacharjee, R.N. Shelton, and P. Kleivins, *Temperature-dependent sinusoidal magnetic order in the superconductor $HoMo_6Se_8$* Phys. Rev. Lett. **52** 133 (1984).
- [14] E.B. Sonin, *Coexistence of Superconductivity and Ferromagnetism in Electron and Nuclear Magnets* J. Low Temp. Phys. **110**, Nos. 112, (1998).
- [15] E.B. Sonin, *Domain structure of superconducting ferromagnets* Phys. Rev. B **66**, 100504 (R) (2002). E.B. Sonin, Phys. Rev. Lett. **95**, 269701 (2005); M. Fauré and A.I. Buzdin, *ibid.* **95**, 269702 (2005).
- [16] D. Aoki and J. Flouquet, *Ferromagnetism and Superconductivity in Uranium Compounds* Phys. Soc. Jpn. **81** (2012) 011003.
- [17] M. Tachiki, H. Matsumoto, T. Koyama, and H. Umezawa, *Self-induced vortices in magnetic superconductors* Solid State Commun. **34**, 19 (1980).
- [18] C.G. Kuper, M. Revzen, and A. Ron, *Ferromagnetic Superconductors: A Vortex Phase in Ternary Rare-Earth Compounds* Phys. Rev. Lett. **44**, 1545 (1980).
- [19] H.S. Greenside, E.I. Blount, and C. M. Varma, *Possible Coexisting Superconducting and Magnetic States* Phys. Rev. Lett. **46**, 49 (1981).
- [20] T.K. Ng and C.M. Varma, *Spontaneous Vortex Phase Discovered?* Phys. Rev. Lett. **78**, 330 (1997); T.K. Ng and C.M. Varma, *Spin and vortex dynamics and electromagnetic propagation in the spontaneous vortex phase* Phys. Rev. B **58**, 11624 (1998).
- [21] E.B. Sonin and I. Felner, *Spontaneous vortex phase in a superconducting weak ferromagnet* Phys. Rev. B **57** (1998) R14000 (R).
- [22] P.C. Canfield, S.L. Bud'ko, B.K. Cho, *Possible co-existence of superconductivity and weak ferromagnetism in $ErNi_2B_2C$* Physica C **262**, 249 (1996).
- [23] H. Kawano, H. Takeya, H. Yoshizawa, K. Kadowaki, *Weak ferromagnetic ordering in the superconducting state of $ErNi_2^{11}B_2C$* J. Phys. Chem. Solids **60**, 1053 (1999); H. Kawano-Furukawa, Y. Ishida, F. Yano, R. Nagatomo, A. Noda, T. Nagata, S. Ohira-Kawamura, C. Kobayashi, H. Yoshizawa, K. Littrell, B.L. Winn, N. Furukawa, H. Takeya, *Creation of vortices by ferromagnetic order in $ErNi_2B_2C$* Physica C **470**, 716 (2010).
- [24] D. Wulferding, I. Yang, J. Yang, M. Lee, H.C. Choi, S.L. Bud'ko, P.C. Canfield, H.W. Yeom, and J. Kim, *Spatially resolved penetration depth measurements and vortex manipulation in the ferromagnetic superconductor $ErNi_2B_2C$* Phys. Rev. B **92**, 014517 (2015).
- [25] H. Bluhm, S.E. Sebastian, J.W. Guikema, I.R. Fisher, and K.A. Moler, *Scanning Hall probe imaging of $ErNi_2B_2C$* Phys. Rev. B **73**, 014514 (2006).
- [26] U. Krey, *Micromagnetic Theory of Ferromagnetic Superconductors* Int. J. Magn. **3**, 65 (1972).
- [27] M. Fauré and A.I. Buzdin, *Domain Structure in a Superconducting Ferromagnet* Phys. Rev. Lett. **94**, 187202 (2005).
- [28] V.H. Dao, S. Burdin, and A. Buzdin, *Size of stripe domains in a superconducting ferromagnet* Phys. Rev. B **84**, 134503 (2011).
- [29] I.M. Khaymovich, A.S. Mel'nikov, and A.I. Buzdin, *Phase transitions in the domain structure of ferromagnetic superconductors* Phys. Rev. B **89** 094524 (2014).
- [30] Z. Ren, Q. Tao, S. Jiang, C. M. Feng, C. Wang, J. H. Dai, G. H. Cao, and Z.-A. Xu, *Superconductivity Induced by Phosphorus Doping and Its Coexistence with Ferromagnetism in $EuFe_2(As_{0.7}P_{0.3})_2$* Phys. Rev. Lett. **102**, 137002 (2009).
- [31] H.S. Jeevan, D. Kasinathan, H. Rosner, and P. Gegenwart, *Interplay of antiferromagnetism, ferromagnetism, and superconductivity in $EuFe_2(As_{1-x}P_x)_2$ single crystals* Phys. Rev. B **83**, 054511 (2011).
- [32] Y. Tokiwa, S.-H. Hübner, O. Beck, H.S. Jeevan, and P. Gegenwart, *Unique phase diagram with narrow superconducting dome in $EuFe_2(As_{1-x}P_x)_2$ due to Eu^{2+} local magnetic moments* Phys. Rev. B **86**, 220505 (R) (2012).

- [33] S. Zapf, H.S. Jeevan, T. Ivek, F. Pfister, F. Klingert, S. Jiang, D. Wu, P. Gegenwart, R. K. Kremer, and M. Dressel, *EuFe₂(As_{1-x}P_x)₂: Reentrant Spin Glass and Superconductivity* Phys. Rev. Lett. **110**, 237002 (2013); S. Zapf, D. Wu, L. Bogani, H. S. Jeevan, P. Gegenwart, and M. Dressel, *Varying Eu²⁺ magnetic order by chemical pressure in EuFe₂(As_{1-x}P_x)₂* Phys. Rev. B **84**, 140503(R) (2011).
- [34] S. Zapf and M. Dressel, *Europium-based iron pnictides: a unique laboratory for magnetism, superconductivity and structural effects* Rep. Prog. Phys. **80**, 016501 (2017).
- [35] A. Pogrebna, T. Mertelj, N. Vujičić, G. Cao, Z.A. Xu, and D. Mihailovic, *Coexistence of ferromagnetism and superconductivity in iron based pnictides: a time resolved magneto-optical study* Sci. Rep. **5**, 7754 (2015).
- [36] I. Nowik, I. Felner, Z. Ren, G. H. Cao, and Z. A. Xu, *Coexistence of ferromagnetism and superconductivity: magnetization and Mössbauer studies of EuFe₂(As_{1-x}P_x)₂*, J. Phys.: Condens. Matter **23**, 065701 (2011).
- [37] T. Goltz, PhD thesis, University of Dresden (2015), *On the electronic phase diagram of Ba_{1-x}K_x(Fe_{1-y}Co_y)₂As₂ and EuFe₂(As_{1-x}P_x)₂ superconductors. A local probe study using Mössbauer spectroscopy and Muon Spin Relaxation.*
- [38] R. Marchand and W. Jeitschko, J. Solid State Chem. **24**, 351 (1978); E. Mörsen, B.D. Mosel, W. Müller-Warmuth, M. Reehuis, W. Jeitschko, *Mössbauer and magnetic susceptibility investigations of strontium, lanthanum and europium transitional metal phosphides with ThCr₂Si₂-type structure* J. Phys. Chem. Solids, **49**, 785 (1988); M. Reehuis and W. Jeitschko, J. Phys. Chem. Solids **51**, 961 (1990); C. Huhnt, W. Schlabitz, A. Wurth, A. Mewis, and M. Reehuis, *First- and second-order phase transitions in ternary europium phosphides with ThCr₂Si₂-type structure* Physica B **252**, 44 (1998).
- [39] X. Xu, W. H. Jiao, N. Zhou, Y. K. Li, B. Chen, C. Cao, J. Dai, A. F. Bangura, and Guanghan Cao, *Electronic nematicity revealed by torque magnetometry in EuFe₂(As_{1-x}P_x)₂* Phys. Rev. B **89**, 104517 (2014).
- [40] W.A. Fertig, D.C. Johnston, L.E. DeLong, R.W. McCallum, M.B. Maple and B.T. Matthias, *Destruction of superconductivity at the onset of long-range magnetic order in the compound ErRh₄B₄*, Phys. Rev. Lett. **38**, 987 (1977).
- [41] W.-H. Jiao, Q. Tao, Z. Ren, Y. Liu, G.-H. Cao, *Evidence of Spontaneous Vortex Ground State in An Iron-Based Ferromagnetic Superconductor* npj Quantum Materials **2**, 50 (2017). (Preprint at arXiv: 1707.08420).
- [42] Wen-He Jiao, Yi Liu, Zhang-Tu Tang, Yu-Ke Li, Xiao-Feng Xu, Zhi Ren, Zhu-An Xu, and Guang-Han Cao, *Peculiar properties of the ferromagnetic superconductor Eu(Fe_{0.91}Rh_{0.09})₂As₂* Supercond. Sci. Technol. **30**, 025012 (2017).
- [43] E.B. Sonin, *Comment on "Ferromagnetic film on a superconducting substrate"* Phys. Rev. B **66**, 136501 (2002).
- [44] K. Hashimoto, M. Yamashita, S. Kasahara, Y. Senshu, N. Nakata, S. Tonegawa, K. Ikada, A. Serafin, A. Carrington, T. Terashima, H. Ikeda, T. Shibauchi, and Y. Matsuda, *Line nodes in the energy gap of superconducting BaFe₂(As_{1-x}P_x)₂ single crystals as seen via penetration depth and thermal conductivity* Phys. Rev. B **81**, 220501 (R) (2010); K. Hashimoto, K. Cho, T. Shibauchi, S. Kasahara, Y. Mizukami, R. Katsumata, Y. Tsuruhara, T. Terashima, H. Ikeda, M.A. Tanatar, H. Kitano, N. Salovich, R.W. Giannetta, P. Walmsley, A. Carrington, R. Prozorov, and Y. Matsuda, *A Sharp Peak of the Zero-Temperature Penetration Depth at Optimal Composition in BaFe₂(As_{1-x}P_x)₂* Science **336**, 1554 (2012).
- [45] D. Neubauer, A.V. Pronin, S. Zapf, J. Merz, H. S. Jeevan, W.-H. Jiao, P. Gegenwart, G.-H. Cao, and M. Dressel, *Optical properties of superconducting EuFe₂(As_{1-x}P_x)₂* Phys. Status Solidi B **254**, No. 1, 1600148 (2017); D. Wu, G. Chanda, H.S. Jeevan, P. Gegenwart, and M. Dressel, *Optical investigations of chemically pressurized EuFe₂(As_{1-x}P_x)₂: An s-wave superconductor with strong interband interactions* Phys. Rev. B **83**, 100503(R) (2011).
- [46] A. Hubert and R. Schäfer, *Magnetic Domains. The Analysis of Magnetic Microstructures*, Springer-Verlag, Berlin, Heidelberg, New York (1998), 720 pp.
- [47] S. Nandi, W.T. Jin, Y. Xiao, Y. Su, S. Price, D.K. Shukla, J. Strempler, H.S. Jeevan, P. Gegenwart, and Th. Brückel, *Coexistence of superconductivity and ferromagnetism in P-doped EuFe₂As₂* Phys. Rev. B **89**, 014512 (2014).
- [48] I.S. Veshchunov, L.Ya. Vinnikov, V.S. Stolyarov, N. Zhou, Z.X. Shi, X.F. Xu, S.Yu. Grebenchuk, D.S. Baranov, I.A. Golovchanskiy, S. Pyon, Yue Sun, Wenhe Jiao, Guanghan Cao, T. Tamegai, A.A. Golubov, *Visualization of the magnetic flux structure in phosphorus-doped EuFe₂As₂ single crystals* JETP Lett. **105**, 98 (2017). (Preprint at arXiv: 1703.02235).
- [49] V. Vlasko-Vlasov, A. Buzdin, A. Mel'nikov, U. Welp, D. Rosenmann, L. Uspenskaya, V. Fratello, and W. Kwok, *Domain structure and magnetic pinning in ferromagnetic/superconducting hybrids* Phys. Rev. B **85**, 064505 (2012).
- [50] Z. Guguchia, A. Shengelaya, A. Maisuradze, L. Howald, Z. Bukowski, M. Chikovani, H. Luetkens, S. Katrych, J. Karpinski, H. Keller, *Muon-Spin Rotation and Magnetization Studies of Chemical and Hydrostatic Pressure Effects in EuFe₂(As_{1-x}P_x)₂* J. Supercond. Nov. Magn. **26**, 285 (2013).
- [51] S. Nandi, W.T. Jin, Y. Xiao, Y. Su, S. Price, W. Schmidt, K. Schmalzl, T. Chatterji, H.S. Jeevan, P. Gegenwart, and Th. Brückel, *Magnetic structure of the Eu²⁺ moments in superconducting EuFe₂(As_{1-x}P_x)₂ with x = 0.19* Phys. Rev. B **90**, 094407 (2014).
- [52] V.K. Anand, D.T. Adroja, A. Bhattacharyya, U.B. Paramanik, P. Manuel, A.D. Hillier, D. Khalyavin, and Z. Hossain, *μSR and neutron diffraction investigations on the reentrant ferromagnetic superconductor Eu(Fe_{0.86}Ir_{0.14})₂As₂* Phys. Rev. B **91**, 094427 (2015).
- [53] K. Kawashima, T. Kinjo, T. Nishio, S. Ishida, H. Fujihisa, Y. Gotoh, K. Kihou, H. Eisaki, Y. Yoshida, and A. Iyo, *Superconductivity in Fe-Based Compound EuFe₄As₄ (A = Rb and Cs)* J. Phys. Soc. Jpn. **85**, 064710 (2016).
- [54] Y. Liu, Y.-B. Liu, Z.-T. Tang, H. Jiang, Z.-C. Wang, A. Ablimit, W.-H. Jiao, Q. Tao, C.-M. Feng, Z.-A. Xu, and G.-H. Cao, *Superconductivity and ferromagnetism in hole-doped RbEuFe₄As₄* Phys. Rev. B **93**, 214503 (2016).
- [55] Y. Liu, Y.-B. Liu, Q. Chen, Z.-T. Tang, W.-H. Jiao, Q. Tao, Z.-A. Xu, and G.-H. Cao, *A New Ferromagnetic Superconductor: CsEuFe₄As₄* Sci. Bull. **61**(15):1213 (2016).
- [56] A. Iyo, K. Kawashima, T. Kinjo, T. Nishio, S. Ishida, H. Fujihisa, Y. Gotoh, K. Kihou, H. Eisaki, and Y. Yoshida, *New-Structure-Type Fe-Based Superconductors: CaAFe₄As₄ (A = K, Rb, Cs) and SrAFe₄As₄ (A = Rb, Cs)* J. Am. Chem. Soc. **138**, 3410 (2016).
- [57] W.R. Meier, T. Kong, U.S. Kaluarachchi, V. Taufour, N.H. Jo, G. Drachuck, A.E. Böhrer, S.M. Saunders, A. Sapkota,

- A. Kreyssig, M.A. Tanatar, R. Prozorov, A.I. Goldman, F.F. Balakirev, A. Gurevich, S.L. Bud'ko, and P.C. Canfield, *Anisotropic thermodynamic and transport properties of single-crystalline $\text{CaKFe}_4\text{As}_4$* Phys. Rev. B **94**, 064501 (2016); K. Cho, A. Fente, S. Teknowijoyo, M.A. Tanatar, K.R. Joshi, N.M. Nusran, T. Kong, W.R. Meier, U. Kaluarachchi, I. Guillaumòn, H. Suderow, S.L. Bud'ko, P.C. Canfield, and R. Prozorov, *Nodeless multiband superconductivity in stoichiometric single-crystalline $\text{CaKFe}_4\text{As}_4$* Phys. Rev. B **95**, 100502 (R) (2017); A. Fente, W.R. Meier, T. Kong, V.G. Kogan, S.L. Bud'ko, P.C. Canfield, I. Guillaumòn, H. Suderow, *Vortices in two-effective-band, stoichiometric high T_c $\text{CaKFe}_4\text{As}_4$ superconductor* Preprint at arXiv: 1608.00605v1.
- [58] R. Hu, S.L. Bud'ko, W.E. Straszheim, and P.C. Canfield, *Phase diagram of superconductivity and antiferromagnetism in single crystals of $\text{Sr}(\text{Fe}_{1-x}\text{Co}_x)_2\text{As}_2$ and $\text{Sr}_{1-y}\text{Eu}_y(\text{Fe}_{0.88}\text{Co}_{0.12})_2\text{As}_2$* Phys. Rev. B **83**, 094520 (2011).
- [59] S. Zapf, PhD thesis, University of Stuttgart (2015), *Optical and Magnetization Studies on Europium Based Iron Pnictides*.
- [60] L.D. Landau and E.M. Lifshitz, *Electrodynamics of Continuous Media* (Pergamon Press, Oxford, 1984).
- [61] Sôshin Chikazumi, *Physics of ferromagnetism*, English ed. prepared with the assistance of C.D. Graham, Jr. - 2nd ed. Oxford University Press, (1997).
- [62] J.M.D. Coey, *Magnetism and Magnetic Materials*, Cambridge University Press, N.Y., (2010).
- [63] C. Kittel, Phys. Rev. **70** (1946) 965.
- [64] L. N. Bulaevskii, and V. L. Ginzburg, *Temperature dependence of the shape of the domain wall in ferromagnetics and ferroelectrics* Zh. Eksp. Teor. Fiz. **45**, 772 (1963) [Sov. Phys. JETP **18**, 530 (1964)].